



THE UNIVERSITY *of* EDINBURGH

Edinburgh Research Explorer

## An integrated pan-tropical biomass map using multiple reference datasets

### Citation for published version:

Avitabile, V, Herold, M, Heuvelink, GBM, Lewis, SL, Phillips, OL, Asner, GP, Armston, J, Asthon, P, Banin, L, Bayol, N, Berry, N, Boeckx, P, de Jong, B, DeVries, B, Girardin, C, Kearsley, E, Lindsell, JA, Lopez-Gonzalez, G, Lucas, R, Malhi, Y, Morel, A, Mitchard, E, Nagy, L, Qie, L, Quinones, M, Ryan, C, Slik, F, Sunderland, T, Vaglio Laurin, G, Valentini, R, Verbeeck, H, Wijaya, A & Willcock, S 2016, 'An integrated pan-tropical biomass map using multiple reference datasets', *Global Change Biology*, vol. 22, no. 4, pp. 1406-1420. <https://doi.org/10.1111/gcb.13139>

### Digital Object Identifier (DOI):

[10.1111/gcb.13139](https://doi.org/10.1111/gcb.13139)

### Link:

[Link to publication record in Edinburgh Research Explorer](#)

### Document Version:

Peer reviewed version

### Published In:

Global Change Biology

### General rights

Copyright for the publications made accessible via the Edinburgh Research Explorer is retained by the author(s) and / or other copyright owners and it is a condition of accessing these publications that users recognise and abide by the legal requirements associated with these rights.

### Take down policy

The University of Edinburgh has made every reasonable effort to ensure that Edinburgh Research Explorer content complies with UK legislation. If you believe that the public display of this file breaches copyright please contact [openaccess@ed.ac.uk](mailto:openaccess@ed.ac.uk) providing details, and we will remove access to the work immediately and investigate your claim.



# **An integrated pan-tropical biomass map using multiple reference datasets**

(PAN-TROPICAL FUSED BIOMASS MAP)

Avitabile V.<sup>1</sup>, Herold M.<sup>1</sup>, Heuvelink G.B.M.<sup>1</sup>, Lewis S.L.<sup>2,3</sup>, Phillips O.L.<sup>2</sup>, Asner G.P.<sup>4</sup>,  
Armston J.<sup>5,6</sup>, Asthon P.<sup>7,8</sup>, Banin L.F.<sup>9</sup>, Bayol N.<sup>10</sup>, Berry N.<sup>11</sup>, Boeckx P.<sup>12</sup>, de Jong B.<sup>13</sup>,  
DeVries B.<sup>1</sup>, Girardin C.<sup>14</sup>, Kearsley E.<sup>12,15</sup>, Lindsell J.A.<sup>16</sup>, Lopez-Gonzalez G.<sup>2</sup>, Lucas R.  
<sup>17</sup>, Malhi Y.<sup>14</sup>, Morel A.<sup>14</sup>, Mitchard E.<sup>11</sup>, Nagy L.<sup>18</sup>, Qie L.<sup>2</sup>, Quinones M.<sup>19</sup>, Ryan C.M.<sup>11</sup>,  
Slik F.<sup>20</sup>, Sunderland, T.<sup>21</sup>, Vaglio Laurin G.<sup>22</sup>, Valentini R.<sup>23</sup>, Verbeeck H.<sup>12</sup>, Wijaya A.<sup>21</sup>,  
Willcock S.<sup>24</sup>

1. Wageningen University, the Netherlands; 2. University of Leeds, UK; 3. University  
College London, UK; 4. Carnegie Institution for Science, USA; 5. The University of  
Queensland, Australia; 6. Information Technology and Innovation, Australia; 7. Harvard  
University, UK; 8. Royal Botanic Gardens, UK; 9. Centre for Ecology and Hydrology, UK;  
10. Foret Ressources Management, France; 11. University of Edinburgh, UK; 12. Ghent  
University, Belgium; 13. Ecosur, Mexico; 14. University of Oxford, UK; 15. Royal Museum  
for Central Africa, Belgium; 16. The RSPB Centre for Conservation Science, UK; 17. The  
University of New South Wales, Australia; 18. Universidade Estadual de Campinas, Brazil;  
19. SarVision, the Netherlands; 20. Universiti Brunei Darussalam, Brunei; 21. Center for  
International Forestry Research, Indonesia; 22. Centro Euro-Mediterraneo sui Cambiamenti  
Climatici, Italy; 23. Tuscia University, Italy; 24. University of Southampton, UK

Correspondence: Valerio Avitabile, tel. +31 317482092, email: [valerio.avitabile@wur.nl](mailto:valerio.avitabile@wur.nl)

Keywords: aboveground biomass, carbon cycle, forest plots, tropical forest, forest inventory,  
REDD+, satellite mapping, remote sensing

Type of paper: Primary Research Article

**26 Abstract**

27 We combined two existing datasets of vegetation aboveground biomass (AGB) (Saatchi et al.,  
28 2011; Baccini et al., 2012) into a pan-tropical AGB map at 1-km resolution using an  
29 independent reference dataset of field observations and locally-calibrated high-resolution  
30 biomass maps, harmonized and upscaled to 14,477 1-km AGB estimates. Our data fusion  
31 approach uses bias removal and weighted linear averaging that incorporates and spatializes  
32 the biomass patterns indicated by the reference data. The method was applied independently  
33 in areas (strata) with homogeneous error patterns of the input (Saatchi and Baccini) maps,  
34 which were estimated from the reference data and additional covariates. Based on the fused  
35 map, we estimated AGB stock for the tropics (23.4 N – 23.4 S) of 375 Pg dry mass, 9% - 18%  
36 lower than the Saatchi and Baccini estimates. The fused map also showed differing spatial  
37 patterns of AGB over large areas, with higher AGB density in the dense forest areas in the  
38 Congo basin, Eastern Amazon and South-East Asia, and lower values in Central America and  
39 in most dry vegetation areas of Africa than either of the input maps. The validation exercise,  
40 based on 2,118 estimates from the reference dataset not used in the fusion process, showed  
41 that the fused map had a RMSE 15 – 21% lower than that of the input maps and, most  
42 importantly, nearly unbiased estimates (mean bias 5 Mg dry mass ha<sup>-1</sup> vs. 21 and 28 Mg ha<sup>-1</sup>  
43 for the input maps). The fusion method can be applied at any scale including the policy-  
44 relevant national level, where it can provide improved biomass estimates by integrating  
45 existing regional biomass maps as input maps and additional, country-specific reference  
46 datasets.

47

48

## 49 **Introduction**

50 Recently, considerable efforts have been made to better quantify the amounts and spatial  
51 distribution of aboveground biomass (AGB), a key parameter for estimating carbon emissions  
52 and removals due to land-use change, and related impacts on climate (Saatchi et al., 2011;  
53 Baccini et al., 2012; Harris et al., 2012; Houghton et al., 2012; Mitchard et al., 2014; Achard  
54 et al., 2014). Particular attention has been given to the tropical regions, where uncertainties  
55 are higher (Pan et al., 2011; Ziegler et al., 2012; Grace et al., 2014). In addition to ground  
56 observations acquired by research networks or for forest inventory purposes, several AGB  
57 maps have been recently produced at different scales, using a variety of empirical modelling  
58 approaches based on remote sensing data calibrated by field observations (e.g., Goetz et al.,  
59 2011; Birdsey et al., 2013). AGB maps at moderate resolution have been produced for the  
60 entire tropical belt by integrating various satellite observations (Saatchi et al., 2011; Baccini et  
61 al., 2012), while higher resolution datasets have been produced at local or national level using  
62 medium-high resolution satellite data (e.g., Avitabile et al., 2012; Cartus et al., 2014),  
63 sometimes in combination with airborne Light Detection and Ranging (LiDAR) data (Asner  
64 et al., 2012a, 2012b, 2013, 2014a). The various datasets often have different purposes:  
65 research plots provide a detailed and accurate estimation of AGB (and other ecological  
66 parameters or processes) at the local level, forest inventory networks use a sampling approach  
67 to obtain statistics of biomass stocks (or growing stock volume) per forest type at the sub-  
68 national or national level, while high-resolution biomass maps can provide detailed and  
69 spatially explicit estimates of AGB density to assist natural resource management, and large  
70 scale coarse-resolution datasets depict AGB distribution for global-scale carbon accounting  
71 and modelling.

72

73 In the context of the United Nations mechanism for Reducing Emissions from Deforestation  
74 and forest Degradation (REDD+), emission estimates obtained from spatially explicit biomass  
75 datasets may be favoured over those based on mean values derived from plot networks. This  
76 preference stems from the fact that plot networks are not designed to represent land cover  
77 change events, which usually do not occur randomly and may affect forests with biomass  
78 density systematically different from the mean value (Baccini and Asner, 2013). With very  
79 few tropical countries having national AGB maps or reliable statistics on forest carbon stocks,  
80 regional maps may provide advantages compared to the use of default mean values (e.g.,  
81 IPCC (2006) Tier 1 values) to assess emissions from deforestation, as long as their accuracy is  
82 reasonable and their estimates are not affected by systematic errors (Avitabile et al., 2011).  
83 These conditions are difficult to assess, however, since rigorous validation of regional AGB  
84 maps remains problematic, given their large area coverage and large mapping unit (Mitchard  
85 et al., 2013), while ground observations are only available for a limited number of small  
86 sample areas.

87

88 The comparison of two recent pan-tropical AGB maps (Saatchi et al., 2011; Baccini et al.,  
89 2012) revealed substantial differences between the two products (Mitchard et al., 2013).  
90 Further comparison with ground observations and high-resolution maps also highlighted  
91 notable differences in AGB patterns at regional scales (Baccini and Asner, 2013; Hills et al.,  
92 2013; Mitchard et al., 2014). Such comparisons have stimulated a debate over the use and  
93 capabilities of different types of biomass products (Saatchi et al., 2014; Langner et al., 2014)  
94 and have highlighted both the importance and sometimes the lack of integration of different  
95 datasets. On one hand, the two pan-tropical maps are consistent in terms of methodology  
96 because both use the same primary data source (GLAS LiDAR) alongside a similar modelling  
97 approach to upscale the LiDAR data to larger scales. Moreover, they have the advantage of

98 being calibrated using hundreds of thousands of AGB estimates derived from height metrics  
99 computed by a spaceborne LiDAR sensor distributed over the tropics. However, such maps  
100 are based on remotely sensed variables that do not directly measure AGB, but are sensitive to  
101 canopy cover and canopy height parameters that do not fully capture the AGB variability of  
102 complex tropical forests. Furthermore, both products assume global or continental allometric  
103 relationships in which AGB varies only with stand height, and further errors are introduced by  
104 upscaling the calibration data to the coarser satellite data. On the other hand, ground plots use  
105 allometric equations to estimate AGB at individual tree level using directly measurable  
106 parameters such as diameter, height and species identity (hence wood density). However, they  
107 have limited coverage, are not error-free, and compiling various datasets over large areas is  
108 made more complex due to differing sampling strategies (e.g., stratification of landscapes,  
109 plot size, minimum diameter of trees measured). Considering the rapid increase of biomass  
110 observations at different scales and the different capabilities and limitations of the various  
111 datasets, it is becoming more and more important to identify strategies that are capable of  
112 making best use of existing information and optimally integrate various data sources for  
113 improved large area AGB assessment (e.g., see Willcock et al., 2012).

114

115 In the present study, we compiled existing ground observations and locally-calibrated high-  
116 resolution biomass maps to obtain a high-quality AGB reference dataset for the tropical  
117 region (Objective 1). This reference dataset was used to assess two existing pan-tropical AGB  
118 maps (Objective 2) and to combine them in a fused map that optimally integrates the two  
119 maps, based on the method presented by Ge et al. (2014) (Objective 3). Lastly, the fused map  
120 was assessed and compared to known AGB stocks and patterns across the tropics (Objective  
121 4).

122

123 Overall, the approach consisted of pre-processing, screening and harmonizing the pan-tropical  
124 AGB maps (called ‘input maps’), the high-resolution AGB maps (called ‘reference maps’)  
125 and the field plots (called ‘reference plots’; ‘reference dataset’ refers to the maps and plots  
126 combined) to a common spatial resolution and geospatial reference system (Figure 1). The  
127 input maps were combined using bias removal and weighted linear averaging (‘fusion’). The  
128 fusion model was applied independently to areas associated with different error patterns of the  
129 input maps (called ‘error strata’), which were estimated from the reference data and additional  
130 covariates (called ‘covariate maps’). The reference dataset included only a subset of the  
131 reference maps (i.e., the cells with highest confidence) and if a stratum was lacking reference  
132 data (‘reference data gaps’), additional data were extracted from the reference maps  
133 (‘consolidation’). The fused map was validated using independent data and its uncertainty  
134 quantified using model parameters. In this study, the terms AGB refers to aboveground live  
135 woody biomass and is reported in units of Mg dry mass ha<sup>-1</sup>. The fused map and the  
136 corresponding reference dataset can be freely downloaded from  
137 [www.wageningenur.nl/grsbiomass](http://www.wageningenur.nl/grsbiomass).

138

139

140

141

142

143

144

145

146

147

## 148 **Materials and methods**

### 149 *Input maps*

150 The input maps used for this study were the two pan-tropical datasets published by Saatchi et  
151 al. (2011) and Baccini et al. (2012), hereafter referred to as the “Saatchi” and “Baccini” maps  
152 individually, or as “input” maps collectively. The Baccini map was provided in MODIS  
153 sinusoidal projection with a spatial resolution of 463 m while the Saatchi map was in a  
154 geographic projection (WGS-84) at 0.00833 degrees (approximately 1 km) pixel size. The  
155 two datasets were harmonized by first projecting the Baccini map to the coordinate system of  
156 the Saatchi map using the Geospatial Data Abstraction Library ([www.gdal.org](http://www.gdal.org)) and then  
157 aggregating it to match the spatial resolution and grid of the Saatchi map. Spatial aggregation  
158 was performed by computing the mean value of the pixels whose centre was located within  
159 each 1-km cell of the Saatchi map. Resampling was then undertaken using the nearest  
160 neighbor method.

161

### 162 *Reference dataset*

163 The reference dataset comprised individual tree-based field data and high-resolution AGB  
164 maps independent from the input maps. The field data included AGB estimates derived from  
165 field measurement of tree parameters and allometric equations. The AGB maps included high-  
166 resolution ( $\leq 100$  m) datasets derived from satellite data using empirical models calibrated  
167 and validated using local ground observations and, in some cases, airborne LiDAR  
168 measurements. Given the variability of procedures used to acquire and produce the various  
169 datasets, they were first screened according to a set of quality criteria to select only the most  
170 reliable AGB estimates, and then pre-processed to be harmonized with the pan-tropical AGB  
171 maps in terms of spatial resolution and observed variables. Field and map datasets providing  
172 aboveground carbon density were converted to AGB units using the same coefficients used



173 for their original conversion from biomass to carbon. The sources and characteristics of the  
174 reference data are listed in the Supplementary Information (Tables S8 - S11).

175

## 176 **Data screening and pre-processing**

### 177 *Reference field data*

178 The reference field data were measurements from forest inventory plots for which accurate  
179 geolocation and biomass estimates were available. Pre-processing of the data consisted of a 2-  
180 step screening and a harmonization procedure. A preliminary screening selected only the  
181 ground data that satisfied the following criteria: (1) they estimated AGB for all living trees  
182 with diameter at breast height  $\geq 5$ -10 cm; (2) they were acquired on or after the year 2000; (3)  
183 they were not used to calibrate the LiDAR-AGB relationships of the input maps; and (4) their  
184 plot coordinates were measured using a GPS. Since the taxonomic identities of trees strongly  
185 indicate wood density, and hence stand-level biomass (e.g., Baker et al., 2004; Mitchard et al.  
186 2014), plots were only selected if tree AGB was estimated using at least tree diameter and  
187 wood density as input parameters. Datasets were excluded if they did not conform to these  
188 requirements or did not provide clear information on the biomass pool measured, the tree  
189 parameters measured in the field, the allometric model applied, the year of measurement or  
190 the plot geolocation and extent. Next, the plot data were projected to the geographic reference  
191 system WGS-84 and harmonized with the input maps by averaging the AGB values located  
192 within the same 1-km pixel if there was more than one plot per pixel, or by directly attributing  
193 the plot AGB to the respective pixel if there was only one plot per pixel. Field plots not fully  
194 located within one pixel were attributed to the map cell where the majority of the plot area  
195 (i.e., the plot centroid) was located.

196

197 Lastly, the representativeness of the plot over the 1-km pixels was considered, and the ground  
198 data were further screened to discard plots not representative of the map cells in terms of  
199 AGB density. More specifically, since the two input maps in their native reference systems  
200 are not aligned and therefore their pixels do not correspond to the same geographic area, the  
201 plot representativeness was assessed on the area of both pixels (identified before the map  
202 resampling). The representativeness was evaluated on the basis of the homogeneity of the tree  
203 cover and crown size within the pixel, determined through visual interpretation of high-  
204 resolution images provided on the Google Earth platform. If the tree cover and tree crowns  
205 were not homogeneous over at least 90% of the pixel area, the plots located within the pixel  
206 were discarded (Fig. S1). In addition, if subsequent Google Earth images indicated that forest  
207 change processes (e.g., deforestation or regrowth) occurred in the period between the field  
208 measurement and the reference years of the input maps, the corresponding plots were  
209 discarded.

210

#### 211 *Reference biomass maps*

212 The reference biomass maps consisted of high-resolution local or national AGB maps  
213 published in the scientific literature. Maps providing AGB estimates grouped in classes (e.g.,  
214 Willcock et al., 2012) were not used since the class values represent the mean AGB over large  
215 areas, usually spanning multiple strata used in the present study (see ‘Stratification approach’).  
216 The reference AGB maps were first pre-processed to match the input maps through re-  
217 projection, aggregation and resampling using the same procedures described for the pre-  
218 processing of the Baccini map. Then, only the cells with largest confidence (i.e., lowest  
219 uncertainty) were selected from the maps. Since uncertainty maps were usually not available,  
220 and considering that the reference maps were based on empirical models, the map cells with  
221 greatest confidence were assumed to be those in correspondence of the training data (field

222 plots and/or LiDAR data). When the locations of the training data were not available, random  
223 pixels were extracted from the maps. For maps based only on radar or optical data, whose  
224 signals saturate above a certain AGB density value, only pixels below such a threshold were  
225 considered. In order to compile a reference database that was representative of the area of  
226 interest and well-balanced among the various input datasets (as defined in ‘Consolidation of  
227 the reference dataset’), the amount of reference data extracted from the AGB maps was  
228 proportional to their area and not greater than the amount of samples provided by the field  
229 datasets representing a similar area. In the case where maps with extensive training areas  
230 provided a disproportionate number of reference pixels, a further screening selected only the  
231 areas underpinned by the largest amount of training data.

232

### 233 **Consolidation of the reference dataset**

234 Considering that the modelling approach used in this study is applied independently by  
235 stratum (which represent areas with homogeneous error structure in both input maps; see  
236 ‘Stratification approach’) and is sensitive to the characteristics of the reference data (see  
237 ‘Modelling approach’), each stratum requires that calibration data are relatively well-balanced  
238 between the various reference datasets. Specifically, if a stratum contains few calibration data,  
239 the model becomes more sensitive to outliers, while if a reference dataset is much larger than  
240 the others, the model is more strongly determined by the dominant dataset. For these reasons,  
241 for the strata where the reference dataset was under-represented or un-balanced, it was  
242 consolidated by additional reference data taken from the reference AGB maps, if available.  
243 The reference data were considered insufficient if a stratum had less than half of the average  
244 reference data per stratum, and were considered un-balanced if a single dataset provided more  
245 than 75% of the reference data of the whole stratum and it was not representative of more than  
246 75% of its area. In such cases, additional reference data were randomly extracted from the

247 reference AGB maps that did not provide more than 75% of the reference data. The amount of  
248 data to be extracted from each map was computed in a way to obtain a reference dataset with  
249 an average number of reference data per stratum and not dominated by a single dataset. If  
250 necessary, additional training data representing areas with no AGB (e.g., bare soil) were  
251 included, using visual analysis of Google Earth images to identify locations without  
252 vegetation.

253

#### 254 **Selected reference data**

255 The AGB reference dataset compiled for this study consisted of 14,477 1-km reference pixels,  
256 distributed as follows: 953 in Africa, 449 in South America, 7,675 in Central America, 400 in  
257 Asia and 5,000 in Australia (Fig. 2, Table 1). The reference data were relatively uniformly  
258 distributed among the strata (Table S6) but their amount varied considerably by continent.  
259 The average amount of reference data per stratum ranged from 50 (Asia) to 958 (Central  
260 America) 1-km reference pixels and their variability (computed as standard deviation relative  
261 to the mean) ranged from 25% (South America) to 52% (Central America). The uneven  
262 distribution of reference data across the continents is mostly caused by the availability of  
263 ground observations: as indicated above, in order to have a balanced reference dataset for  
264 each stratum the reference data extracted from AGB maps were limited to the (smaller)  
265 amount of direct field observations. When AGB maps were the only source of data, this  
266 constraint was not occurring and larger datasets could be derived from the maps (i.e., Central  
267 America, Australia).

268

269 The reference data were selected from 18 ground datasets and from 9 high-resolution AGB  
270 maps calibrated by field observations and, in 4 cases, airborne LiDAR data (Table 1). The  
271 field plots used for the calibration of the maps are not included in this section because they

272 were only used to select the reference pixels from the maps. The visual screening of the field  
273 plots removed 35% of the input data (from 6,627 to 4,283) and their aggregation to 1-km  
274 resolution further removed 70% of the reference units derived from field plots (from 4,283 to  
275 1,274), while 10,741 reference pixels were extracted from the high-resolution AGB maps.  
276 The criteria used to select the reference pixels for each map are reported in Table S2. The  
277 consolidation procedure was necessary only for Central America where it added 2,415  
278 reference data, while 47 pixels representing areas with no AGB were identified in Asia (Table  
279 S1). In general, ground observations were mostly discarded in areas characterized by  
280 fragmented or heterogeneous vegetation cover and high biomass spatial variability. In such  
281 contexts, reference data were often acquired from the AGB maps.

282

### 283 ***Stratification approach***

284 Preliminary comparison of the reference data with the input maps showed that the error  
285 variances and biases of the input maps were not spatially homogeneous but varied  
286 considerably in different regions. Since the fusion model used in this study (see ‘Modelling  
287 approach’) is based on bias removal and weighted combination of the input maps, the more  
288 homogeneous the error characteristics in the input maps are, the better they can be reduced by  
289 the model. For this reason, the stratification approach aimed at identifying areas with  
290 homogeneous error structure (hereafter named ‘error strata’) in both input maps. A first  
291 stratification was undertaken based on geographic location (namely Central America, South  
292 America, Africa, Asia and Australia) to reflect the regional allometric relationships between  
293 AGB and tree diameter and height (Feldpausch et al., 2011, 2012). Then, the error strata were  
294 identified for each continent using a two-step process. First, the error maps of the Saatchi and  
295 Baccini maps were predicted separately. Since the AGB estimates of the input maps were  
296 mostly based on optical and LiDAR data that are sensitive to tree cover and tree height, it was

297 assumed that their uncertainties were related to the spatial variation of these parameters. In  
298 addition, the errors of the input maps were found to be linearly correlated with the respective  
299 AGB estimates. For these reasons, the AGB maps themselves, as well as global datasets of  
300 land cover (ESA, 2014a), tree cover (Di Miceli et al., 2014) and tree height (Simard et al.,  
301 2011), were used to predict the map errors using a Random Forest model (Breiman, 2001)  
302 calibrated on the basis of the reference dataset. Second, the error maps of the Saatchi and  
303 Baccini datasets were clustered using the K-Means approach. The use of eight clusters (hence,  
304 eight error strata) was considered a sensible trade-off between homogeneity of the errors of  
305 the input maps and number of reference observations available per stratum, with a larger  
306 number of clusters providing only a marginal increase in homogeneity but leading to a small  
307 number of reference data in some strata (Fig. S2). In areas where the predictors presented no  
308 data (i.e., outside the coverage of the Baccini map) or for classes of the categorical predictor  
309 without reference data (i.e., land cover), the error strata (instead of the error maps) were  
310 predicted using an additional Random Forest model based on predictors without missing  
311 values (i.e., Saatchi map, tree cover and tree height) and 10,000 training data randomly  
312 extracted from the stratification map.

313

314 This method produced a stratification map that identified eight strata for each continent with  
315 homogeneous error patterns in the input maps (Fig. S3). The root mean square error (RMSE)  
316 computed on the Out-Of-Bag data (i.e., data not used for training) of the Random Forest  
317 models that predicted the errors of the input maps ranged between  $22.8 \pm 0.3 \text{ Mg ha}^{-1}$  (Central  
318 America) to  $83.7 \pm 2.5 \text{ Mg ha}^{-1}$  (Africa), with the two models (one for each input map)  
319 achieving similar accuracies in each continent (Table S4, Fig. S4). In most cases the main  
320 predictors of the errors of the input maps were the biomass values of the maps themselves,  
321 followed by tree cover and tree height, while land cover was always the least important

322 predictor (Table S5). Further details on the processing of the input data are provided in the  
323 Supplementary Information.

324

325 The use of a stratification based on the errors of the input maps was compared with  
326 stratifications based on land cover (used by Ge et al., 2014), tree cover and tree height. A  
327 separate stratification map was obtained for each of these alternative variables by aggregation  
328 into eight strata (to maintain comparability with the number of clusters used in the error  
329 strata), and each stratification map was used to develop a specific fused map. The  
330 performance of alternative stratification approaches was assessed by validating the respective  
331 fused maps (see Supplementary Information – Alternative stratification approaches). The  
332 results demonstrated that the stratification based on error modelling and clustering (i.e., the  
333 error strata) produced a fused map with higher accuracy than that of the maps based on other  
334 stratification approaches, and therefore was used in this study (Fig. S5).

335

### 336 *Modelling approach*

#### 337 **The fusion model**

338 The integration of the two input maps was performed with a fusion model based on the  
339 concept presented by Ge et al. (2014) and further developed for this study. The fusion model  
340 consists of bias removal and weighted linear averaging of the input maps to produce an output  
341 with greater accuracy than each of the input maps. The reference AGB dataset described  
342 above was used to calibrate the model and to assess the accuracy of the input and fused maps.  
343 A specific model was developed for each stratum.

344

345 Following Ge et al. (2014), the  $p$  input maps for locations  $s \in D$ , where  $D$  is the geographical  
346 domain of interest common to the input maps, were combined using a weighted linear average:

$$347 \quad (1) \quad f(s) = \sum_{i=1}^p w_i(s) \cdot (z_i(s) - v_i(s))$$

348 where  $f$  is the fused map, the  $w_i(s)$  are weights,  $z_i$  the estimate of the  $i$ -th input map and  $v_i(s)$  is  
 349 the bias estimate. The bias term was computed as the average difference between the input  
 350 map and the reference data for each stratum. The weights were obtained from a statistical  
 351 model that assumes the map estimates  $z_i$  to be the sum of the true biomass  $b_i$  with a bias term  
 352  $v_i$  and a random noise term  $\varepsilon_i$  with zero mean for each location  $s \in D$ . We further assumed that  
 353 the  $\varepsilon_i$  of the input maps are jointly normally distributed with variance-covariance matrix  $C(s)$ .  
 354 Differently from Ge et al. (2014),  $C(s)$  was estimated using a robust covariance estimator as  
 355 implemented by the ‘robust’ package in R (Wang et al., 2014), which uses the Stahel-Donoho  
 356 estimator for strata with fewer than 5,000 observations and the Fast Minimum Covariance  
 357 Determinant estimator for larger strata. Under these assumptions, the variance of the  
 358 estimation error of the fused map  $f(s)$  is minimized by calculating the weights  $w(s)$  as outlined  
 359 by Searle (1971, p. 89):

$$360 \quad (2) \quad w(s)^T = (\mathbf{1}^T C(s)^{-1} \mathbf{1})^{-1} \mathbf{1}^T C(s)^{-1}$$

361 where  $\mathbf{1} = [1, \dots, 1]^T$  is the transpose of the  $p$ -dimensional unit vector. The weights computed  
 362 for each stratum sum to 1, while their values are approximately inversely proportional to the  
 363 error variance of the corresponding input map. Larger weights are assigned to input maps with  
 364 lower error variances, although the covariance between map errors influences the weights as  
 365 well. Overall, the fused map is expected to provide more accurate estimates after bias removal  
 366 and weighted averaging of the input maps. The fusion model assured that the variance of the  
 367 error in the fused map was smaller than that of the input maps (Bates and Granger, 1969),  
 368 especially if the errors associated with these maps were not strongly positively correlated and  
 369 their error variances were close to the smallest error variance. The fusion model can be  
 370 applied to any number of input maps. Where there is only one input map, the model estimates  
 371 and removes its bias and the weights are set equal to 1.



372

**373 The model parameters**

374 The fusion model computed a set of bias and weight parameters for each stratum and  
375 continent on the basis of their respective reference data, and used these for the linear weighted  
376 combination of the input maps (Table S6). Since the stratification approach grouped together  
377 data with similar error patterns, the biases varied considerably among the strata and could  
378 reach values up to  $\pm 200 \text{ Mg ha}^{-1}$ . However, considering the area of the strata, the biases of  
379 both input maps were smaller than  $\pm 45 \text{ Mg ha}^{-1}$  for at least 50% of the area of all continents  
380 and smaller than  $\pm 100 \text{ Mg ha}^{-1}$  for 81% - 98% of the area of all continents.

381

**382 *Post-processing*****383 Predictions outside the coverage of the Baccini map**

384 The Baccini map covers the tropical belt between 23.4 degree north latitude and 23.4 degree  
385 south latitude while the Saatchi map presents a larger latitudinal coverage (Fig. 2). The fusion  
386 model was first applied to the area common to both input maps (Baccini extent) and then  
387 extended to the area where only the Saatchi map is available. In the latter area, the model  
388 focused only on removing the bias of the Saatchi map using the values estimated for the  
389 Baccini extent. The model predictions for the Saatchi extent were mosaicked to those for the  
390 Baccini extent using a smoothing function (inverse distance weight) on an overlapping area of  
391 1 degree within the Baccini extent between the two maps. Water bodies were masked over the  
392 whole study area using the ESA CCI Water Bodies map (ESA, 2014b). The resulting fused  
393 map was projected to an equal area reference system (MODIS Sinusoidal) before computing  
394 the total AGB stocks for each continent, which were obtained by summing the products of the  
395 AGB density of each pixel with their area.

396

### 397 **Assessing AGB in intact and non-intact forest**

398 The AGB estimates of the fused and input maps in forest areas were further investigated  
399 regarding their distribution in ecozones and between intact and non-intact landscapes. Forest  
400 areas were defined as areas dominated by tree cover according to the GLC2000 map  
401 (Bartholomé and Belward, 2005). Ecozones were defined according to the Global Ecological  
402 Zone (GEZ) map for the year 2000 (FAO, 2000). The intact landscapes were defined  
403 according to the Intact Forest Landscape (IFL) map for the year 2000 (Potapov et al., 2008).  
404 On the basis of these datasets, the mean forest AGB density of the fused and input maps were  
405 computed for intact and non-intact landscapes for each continent and major ecozone. To allow  
406 direct comparison of the results among the maps, the analysis was performed only for the area  
407 common to all maps (Baccini extent). In addition, to reduce the impact of spatial inaccuracies  
408 in the maps, only ecozones with IFL intact forest areas larger than 1,000 km<sup>2</sup> were considered.  
409 The mean AGB density of intact and non-intact forests per continent was computed as the  
410 area-weighted mean of the contributing ecozones.

411

### 412 ***Validation and uncertainty***

413 Validation of the fused and input maps was performed by randomly splitting the reference  
414 data into a calibration set (70% of the data) and a validation set (remaining 30%). The ‘final’  
415 fused map presented in Fig. 3 used 100% of the reference data while for validation purposes a  
416 ‘test’ fused map was produced using only the calibration data. The estimates of the ‘test’  
417 fused map, as well as those of the input maps, were compared with the validation data. Note  
418 that validation of the ‘test’ fused map only yields an approximate (i.e., conservative) estimate  
419 of the accuracy of the ‘final’ fused map. In other words, the ‘final’ fused map is likely more  
420 accurate than the ‘test’ fused map because it uses a larger calibration data set. To maintain full  
421 independence, validation data were not used for any step related to the development of the

422 ‘test’ fused map, including production of the stratification map. To account for any potential  
423 impacts of the random selection of validation data, the procedure was repeated 100 times,  
424 computing a new random selection of the calibration and validation datasets with each  
425 iteration. This procedure allowed computing the mean RMSE and assessing its standard  
426 deviation for the fused and input maps.

427

428 The uncertainty of the fused map was computed with respect to model uncertainty, not  
429 including the error sources in the input data (see ‘Discussion’). The model uncertainty  
430 consisted of the expected variance of the error of the fused map (which is assumed to be bias-  
431 free) and was derived for each stratum from  $C(s)$ . The uncertainty was thus estimated per  
432 strata and not at the pixel level. The error variance was converted to an uncertainty map by  
433 reclassifying the stratification map, where the stratum value was converted to the respective  
434 error variance computed for each stratum and continent.

435

436

437

438

439

440

441

442

443

444

445

446

## 447 **Results**

### 448 *Biomass map*

449 The fusion model produced an AGB map at 1-km resolution for the tropical region, with an  
450 extent equal to that of the Saatchi map (Fig. 3). In terms of stocks, the AGB estimates within  
451 the fused map were lower than both input maps at continental level. The total stock of the  
452 fused map for the tropical belt covered by the Baccini map (23.4 N – 23.4 S, see Fig. 2) was  
453 375 Pg dry mass, 9% and 18% lower than the Saatchi (413 Pg) and Baccini (457 Pg)  
454 estimates, respectively. Considering the larger extent of the Saatchi map, the fused map  
455 estimate was 462 Pg, 15% lower than the estimate of the Saatchi map (545 Pg) (Table S7).

456

457 Moreover, the fused map presented spatial patterns that differed substantially from both input  
458 maps (Fig. 4): the AGB estimates were higher than the Saatchi and Baccini maps in the dense  
459 forest areas in the Congo basin, in West Africa, in the north-eastern part of the Amazon basin  
460 (Guyana shield) and in South-East Asia, and lower in Central America and in most dry  
461 vegetation areas of Africa. In the central part of the Amazon basin the fused map showed  
462 lower estimates than the Baccini map and higher estimates than the Saatchi map, while in the  
463 southern part of the Amazon basin these differences were inverted. Similar trends emerged  
464 when comparing the maps separately for intact and non-intact forest ecozones (Supporting  
465 Information). In addition, the average difference between intact and non-intact forests was  
466 larger than that derived from the input maps in Africa and Asia, similar or slightly larger in  
467 South America, and smaller in Central America (Fig. S6).

468

469 According to the fused map, the highest AGB density ( $> 400 \text{ Mg ha}^{-1}$ ) is found in the Guyana  
470 shield, in the central and western part of the Congo basin and in the intact forest areas of  
471 Borneo and Papua New Guinea. The analysis of the distribution of forest AGB in intact and

472 non-intact ecozones showed that the mean AGB density was greatest in intact African (360  
473 Mg ha<sup>-1</sup>) and Asian (335 Mg ha<sup>-1</sup>) forests, followed by intact forests in South America (266  
474 Mg ha<sup>-1</sup>) and Central America (146 Mg ha<sup>-1</sup>) (Fig. S6). AGB in non-intact forests was much  
475 lower in all regions (Africa, 78 Mg ha<sup>-1</sup>; Asia, 211 Mg ha<sup>-1</sup>; South America, 149 Mg ha<sup>-1</sup>; and  
476 Central America, 57 Mg ha<sup>-1</sup>) (Fig. S6).

477

### 478 ***Validation***

479 The validation exercise showed that the fused map achieved a lower RMSE (a decrease of 5 –  
480 74%) and bias (a decrease of 90 – 153%) than the input maps for all continents (Fig. 5). While  
481 the RMSE of the fused map was consistently lower than that of the input maps but still  
482 substantial (87 – 98 Mg ha<sup>-1</sup>) in the largest continents (Africa, South America and Asia), the  
483 mean error (bias) of the fused map was almost null in most cases. Moreover, in the three main  
484 continents the bias of the input maps tended to vary with biomass, with overestimation at low  
485 values and underestimation at high values, while the errors of the fused map were more  
486 consistently distributed (Fig. 6). When computing the error statistics for the pan-tropics  
487 (Baccini extent) as the average of the regional validation results weighted by the respective  
488 area coverage, the mean bias (in absolute terms) for the fused, Saatchi and Baccini maps was  
489 5, 21 and 28 Mg ha<sup>-1</sup> and the mean RMSE was 89, 104 and 112 Mg ha<sup>-1</sup>, respectively (Fig. 5).  
490 The accuracy of the input maps reported above was computed using the validation dataset  
491 (30% of the reference dataset) to be consistent with the accuracy of the fused map. The  
492 accuracy of the input maps was also computed using all reference data and the results (Table  
493 S3) were similar to those based on the validation dataset.

494

### 495 ***Uncertainty map***

496 The uncertainty of the model predictions indicated that the standard deviation of the error of  
497 the fused map for each stratum was in the range 11 - 108 Mg ha<sup>-1</sup>, with largest uncertainties in  
498 areas with largest AGB estimates (Congo basin, Eastern Amazon basin and Borneo). When  
499 computed in relative terms (as a percentage of the AGB estimate), the model uncertainties  
500 presented opposite patterns, with uncertainties larger than the estimates (> 100%) in the low  
501 AGB areas (< 20 Mg ha<sup>-1</sup> on average) of Africa, South America and Central America, while  
502 high AGB forests (> 210 Mg ha<sup>-1</sup> on average) had uncertainties lower than 25% (Fig. 7). The  
503 uncertainty measure derived from  $C(s)$  was computed only when two or more input maps  
504 were available. Hence, it could not be calculated for Australia because the model for this  
505 continent was based on only one input map (Saatchi map).

506

507

508

509

510

511

512

513

514

515

516

517

518

519

## 520 **Discussion**

### 521 *Biomass patterns and stocks emerging from the reference data*

522 The AGB map produced with the fusion approach is largely driven by the reference dataset  
523 and essentially the method is aimed at spatializing the AGB patterns indicated by the  
524 reference data using the support of the input maps. For this reason, great care was taken in the  
525 pre-processing of the reference data, which included a two-step quality screening based on  
526 metadata analysis and visual interpretation, and their consolidation after stratification. As a  
527 result, the reference dataset provides an unprecedented compilation of AGB estimates at 1-km  
528 resolution for the tropical region, covering a wide range of vegetation types, biomass ranges  
529 and ecological regions across the tropics. It includes the most comprehensive and accurate  
530 tropical field plot networks and high-quality maps calibrated with airborne LiDAR, which  
531 provide more accurate estimates compared to those obtained from other sensors (Zolkos et al.,  
532 2013). The main trends present in the fused map emerged from the combination of different  
533 and independent reference datasets and are in agreement with the estimates derived from  
534 long-term research plot networks (Malhi et al., 2006; Phillips et al., 2009; Lewis et al., 2009;  
535 Slik et al., 2010, 2013; Lewis et al., 2013) and high-resolution maps (Asner et al., 2012a,  
536 2012b, 2013, 2014a). Specifically, the AGB patterns in South America represent spatial  
537 trends described by research plot networks in the dense intact and non-intact forests in the  
538 Amazon basin, forest inventory plots collected in the dense forests of Guyana and samples  
539 extracted from AGB maps for Colombia and Peru representing a wide range of vegetation  
540 types, from arid grasslands to humid forests. Similarly, AGB patterns depicted in Africa were  
541 derived from a combination of various research plots in dense undisturbed forest (Gabon,  
542 Cameroon, Democratic Republic of Congo, Ghana, Liberia), inventory plots in forest  
543 concessions (Democratic Republic of Congo), AGB maps in woodland and savannah  
544 ecosystems (Uganda, Mozambique) and research plots and maps in montane forests (Ethiopia,

545 Madagascar). Most vegetation types in Central America, Asia and Australia were also well-  
546 represented by the extensive forest inventory plots (Indonesia, Vietnam and Laos) and high-  
547 resolution maps (Mexico, Panama, Australia).

548

549 In spite of the extensive coverage, the current database is far from being representative of the  
550 AGB variability across the tropics. As a consequence, the model estimates are expected to be  
551 less accurate in contexts not adequately represented. In the case of the fusion approach, this  
552 corresponds to the areas where the input maps present error patterns different than those  
553 identified in areas with reference data: in such areas the model parameters used to correct the  
554 input maps (bias and weight) may not adequately reflect the errors of the input maps and  
555 hence cannot optimally correct them. In particular, deciduous vegetation and heavily  
556 disturbed forest of Africa and South America, and large parts of Asia were lacking quality  
557 reference data. Moreover, even though plot data were spatially distributed over the central  
558 Amazon and the Congo basin, large extents of these two main blocks of tropical forest have  
559 never been measured (cf. maps in Lewis et al., 2013; Mitchard et al., 2014). Considering the  
560 evidence of significant local differences in forest structure and AGB density within the same  
561 forest ecosystems (Kearsley et al., 2013), additional data are needed to strengthen the  
562 confidence of the fused map as well as that of any other AGB map covering the tropical  
563 region. Moreover, a dedicated gap analysis to assess the main regions lacking AGB reference  
564 data and identify priority areas for new field sampling and LiDAR campaigns would be very  
565 valuable for future improved biomass mapping.

566

567 Regarding the AGB stocks, a previous study showed that despite their often very strong local  
568 differences, the two input maps tended to provide similar estimates of total stocks at national  
569 and biome scales and presented an overall net difference of 10% for the pan-tropics (Mitchard



570 et al., 2013). However, such convergence is mostly due to compensation of contrasting  
571 estimates when averaging over large areas. The larger differences with the estimates of the  
572 present study (9% and 18%) suggest an overestimation of the total stocks by the input maps.  
573 This is in agreement with the results of two previous studies that, on the basis of reference  
574 maps obtained by field-calibrated airborne LiDAR data, identified an overestimation of 23% -  
575 42% of total stocks in the Saatchi and Baccini maps in the Colombian Amazon (Mitchard et  
576 al., 2013) and a mean overestimation of about 100 Mg ha<sup>-1</sup> for the Baccini map in the  
577 Colombian and Peruvian Amazon (Baccini and Asner, 2013).

578

579 In general, the AGB density values of the fused map were calibrated and therefore in  
580 agreement with the existing estimates obtained from plot networks and high-resolution maps.  
581 The comparison of mean AGB values in intact and non-intact forests stratified by ecozone  
582 provided further information on the differences between the maps. The mean AGB values of  
583 the fused map in non-intact forests were mostly lower than those of the input maps,  
584 suggesting that in disturbed forests the AGB estimates derived from stand height parameters  
585 retrieved by spaceborne LiDAR (as in the input maps) tend to be higher compared to those  
586 based on tree parameters or very high-resolution airborne LiDAR measurements (as in the  
587 fused map and reference data). This difference occurred especially in Africa, Asia and Central  
588 America while it was less evident in South America and Australia. By contrast, the  
589 differences among the maps for intact forests varied by continent, with the fused map having,  
590 on average, higher mean AGB values in Africa, Asia and Australia, lower values in Central  
591 America, and variable trends within South America, reflecting the different allometric  
592 relationships used by the various datasets in different continents.

593

594 As mentioned above, a larger amount of reference data, ideally acquired based on a clear  
595 statistical sampling design instead of one that is opportunistic, will be required to confirm  
596 such conclusions. While dense sampling of tropical forests using field observations is often  
597 impractical, new approaches combining sufficient ground observations of individual trees at  
598 calibration plots with airborne LiDAR measurements for larger sampling transects would  
599 allow a major increase in the quantity of calibration data. In combination with wall-to-wall  
600 medium resolution satellite data (e.g., Landsat) these may be capable of achieving high  
601 accuracy over large areas (10% - 20% uncertainty at 1-ha scale) while being cost-effective  
602 (e.g., Asner et al., 2013, 2014b). In addition, new technologies, such as Terrestrial Laser  
603 Scanning (TLS), allows for better estimates at ground level (Calders et al., 2015; Gonzalez de  
604 Tanago et al., 2015), considerably reducing the uncertainties of field estimates based on  
605 generalized allometric equations and avoiding destructive sampling. Nevertheless, since  
606 floristic composition influences AGB at multiple scales (e.g., the strong pan-Amazon gradient  
607 in wood density shown by ter Steege et al., 2006) such techniques benefit from extensive and  
608 precise measurements of tree identity in order to determine wood density patterns and to  
609 account for variations in hollow stems and rottenness (Nogueira et al., 2006). Moreover, we  
610 note that the reference data do not include lianas, which may constitute a substantial amount  
611 of woody stems, and their inclusion would allow to obtain more correct estimates of total  
612 AGB of vegetation (Phillips et al., 2002; Schnitzer & Bongers, 2011; Durán & Gianoli, 2013).  
613

#### 614 *Additional error sources*

615 Apart from the uncertainty of the fusion model described above (see 'Uncertainty'), three  
616 other sources of error were identified and assessed in the present approach: i) errors in the  
617 reference dataset; ii) errors due to temporal mismatch between the reference data and the  
618 input maps; iii) errors in the stratification map.

619

**620 Errors in the reference dataset**

621 The reference dataset is not error-free but it inherits the errors present in the field data and  
622 local maps. In addition, additional uncertainties are introduced during the pre-processing of  
623 the data by resampling the maps and upscaling the plot data to 1-km resolution. In particular,  
624 while the geolocation error of the original datasets was considered relatively small ( $< 50$  m)  
625 since plot coordinates were collected using GPS measurements and the AGB maps were  
626 based on satellite data with accurate geolocation (i.e., Landsat, ALOS, MODIS), larger errors  
627 (up to 500 m, half a pixel) could have been introduced with the resampling of the 1-km input  
628 maps. All these error sources were minimized by selecting only the datasets that fulfilled  
629 certain quality criteria and by further screening them through visual analysis of high-  
630 resolution images available on the Google Earth platform, discarding the data not  
631 representative of the respective map pixels. In case of reference data that clearly did not  
632 match with the high-resolution images and/or with the input maps (e.g., reporting no AGB in  
633 dense forest areas or high AGB on bare land), the data were considered as an error in the  
634 reference dataset, a geolocation error in the plots or maps, or it was assumed that a land  
635 change process occurred between the plot measurement and the image acquisition time (see  
636 next paragraph).

637

**638 Errors due to temporal mismatch**

639 The temporal difference of input and reference data introduced some uncertainty in the fusion  
640 model. The input maps refer to the years 2000 – 2001 (Saatchi) and 2007 – 2008 (Baccini)  
641 while the reference data mostly spanned the period 2000 – 2013. Therefore, the differences  
642 between the input maps and the reference data may also be due to a temporal mismatch of the  
643 datasets. However, changes due to deforestation were most likely excluded during the visual

644 selection of the reference data, when high-resolution images showed clear land changes (e.g.,  
645 bare land or agriculture) in areas where the input maps provided AGB estimates relative to  
646 forest areas (or *vice-versa*, depending on the timing of acquisition of the datasets). However,  
647 changes due to forest regrowth and degradation events that did not affect the forest canopy  
648 could not be considered with the visual analysis and may have affected the mismatch  
649 observed between the reference data and the input maps ( $< 58 - 80 \text{ Mg ha}^{-1}$  for 50% of the  
650 cases of the Saatchi and Baccini maps, respectively). Part of the mismatch was in the range of  
651 AGB changes that can be attributed to regrowth ( $1 - 13 \text{ Mg ha}^{-1} \text{ year}^{-1}$ ) (IPCC, 2003) or low-  
652 intensity degradation ( $14 - 100 \text{ Mg ha}^{-1}$ , or 3 - 15% of total stock) (Asner et al., 2010;  
653 Pearson et al., 2014). On the other hand, considering the limited area affected by degradation  
654 (about 20% in the humid tropics) (Asner et al., 2009), the temporal mismatch could be  
655 responsible only for a correspondent part of the differences observed between the reference  
656 data and the input maps. Small additional offsets may also be caused by the documented  
657 secular changes in AGB density within intact tropical forests, which has been increasing by  
658 0.2 - 0.5% per year (Phillips et al., 1998, Chave et al., 2008, Phillips and Lewis, 2014). It  
659 should also be noted that the reference data were used to optimally integrate the input maps,  
660 and in the case of a temporal difference the fused map was 'actualized' to the state of the  
661 vegetation when the reference data were acquired. The reference data were acquired between  
662 2000 and 2013, and their mean acquisition year weighted by their contribution to the fusion  
663 model (by continent) corresponds to the period 2007 - 2010 (2007 in Africa, 2008 in Central  
664 America, 2009 in South America and 2010 in Asia). Therefore the complete fused map cannot  
665 be attributed to a specific year and more generally it represents the first decade of the 2000s.

666

667 **Errors in the stratification map**

668 The errors in the stratification map (i.e., related to the prediction of the errors of the input  
669 maps) were still substantial in some areas and affected the fused map in two ways. First, the  
670 reference data that were erroneously attributed to a certain stratum introduced ‘noise’ in the  
671 estimation of the model parameters (bias and weight), but the impact of these ‘outliers’ was  
672 largely reduced by the use of a robust covariance estimator. Second, erroneous predictions of  
673 the strata caused the use of incorrect model parameters in the combination of the input maps.  
674 The latter is considered to be the main source of error of the fused map and indicates that the  
675 method can achieve improved results if the errors of the input maps can be predicted more  
676 accurately. However, additional analysis showed that, on average, fused maps based on  
677 alternative stratification approaches achieved lower accuracy than the map based on an error  
678 stratification approach (Fig. S5). Therefore, this approach was preferred over a stratification  
679 based on an individual biophysical variable (e.g., tree cover, tree height, land cover or  
680 ecozone).

681

### 682 *Application of the method at national scale*

683 The fusion method presented in this study allows for the optimal integration of any number of  
684 input maps to match the patterns indicated by the reference data. However, the accuracy of the  
685 fused map depends on the availability of reference data representative of the error patterns of  
686 the input maps. While the current reference database does not represent adequately all error  
687 strata for the tropical region, and the model estimates are expected to have lower confidence  
688 in under-represented areas, the proposed method may be applied locally and provide  
689 improved AGB estimates where additional reference data are available. For example, the  
690 fusion method may be applied at national level using existing forest inventory data, research  
691 plots and local maps that cover only part of the country to calibrate global or regional maps,  
692 which provide national coverage but may not be tailored to the country context. Such country-

693 calibrated AGB maps may be used to support natural resource management and national  
694 reporting under the REDD+ mechanism, especially for countries that have limited capacities  
695 to map AGB from remote sensing data (Romijn et al., 2012). Considering the increasing  
696 number of global or regional AGB datasets based on different data and methodologies  
697 expected in the coming years, and that likely there will not be a single ‘best map’ but rather  
698 the accuracy of each will vary spatially, the fusion approach may allow to optimally combine  
699 and adjust available datasets to local AGB patterns identified by reference data.

700

701

702

703

704

705

706

707

708

709

710

711

712

713

714

715

716

717

**718 Acknowledgments**

719 This study was supported by the EU FP7 GEOCARBON (283080) project, by NORAD (grant  
720 agreement no. QZA-10/0468) and AusAID (grant agreement no. 46167) within CIFOR's  
721 Global Comparative Study on REDD+. This work was further supported by the German  
722 Federal Ministry for the Environment, Nature Conservation and Nuclear Safety (BMU)  
723 International Climate Initiative (IKI) through the project "From Climate Research to Action  
724 under Multilevel Governance: Building Knowledge and Capacity at Landscape Scale". Data  
725 were also acquired and/or collated by the Sustainable Landscapes Brazil project supported by  
726 the Brazilian Agricultural Research Corporation (EMBRAPA), the US Forest Service and  
727 USAID, and the US Department of State, Aberystwyth University, the University of New  
728 South Wales (UNSW), and the Queensland Department of Science, Information Technology  
729 and Innovation (DSITI). GP Asner and the Carnegie Airborne Observatory were supported by  
730 the Avatar Alliance Foundation, John D. and Catherine T. MacArthur Foundation, and NSF  
731 grant 1146206. OP, SLL and LQ acknowledge the support of the European Research Council  
732 (T-FORCES), TS, LQ and SLL were supported by CIFOR/USAID; SLL was also supported  
733 by a Philip Leverhulme Prize. LQ thanks the Forestry Department Sarawak, Sabah  
734 Biodiversity Council, State Ministry of Research and Technology (RISTEK) Indonesia for  
735 permissions to carry out the 2013-2014 recensus of long-term forest plots in Borneo (a subset  
736 of which included as Cluster AS16), and Lip Khoon Kho, Sylvester Tan, Haruni Krisnawati  
737 and Edi Mirmanto for field assistance and accessing plot data.

738

739

740

741

742

743 **References**

- 744 Achard F, Beuchle R, Mayaux P et al. (2014) Determination of tropical deforestation rates  
745 and related carbon losses from 1990 to 2010. *Global Change Biology*, **20**, 2540–2554.
- 746 Asner GP, Clark JK, Mascaro J et al. (2012a) High-resolution mapping of forest carbon stocks  
747 in the Colombian Amazon. *Biogeosciences*, **9**, 2683–2696.
- 748 Asner GP, Clark JK, Mascaro J et al. (2012b) Human and environmental controls over  
749 aboveground carbon storage in Madagascar. *Carbon Balance and Management*, **7**, 2.
- 750 Asner GP, Mascaro J, Anderson C et al. (2013) High-fidelity national carbon mapping for  
751 resource management and REDD+. *Carbon balance and management*, **8**, 7.
- 752 Asner GP, Knapp DE, Martin RE et al. (2014a) Targeted carbon conservation at national  
753 scales with high-resolution monitoring. *Proceedings of the National Academy of*  
754 *Sciences*, **111**, E5016–E5022.
- 755 Asner GP, Mascaro J (2014b) Mapping tropical forest carbon: Calibrating plot estimates to a  
756 simple LiDAR metric. *Remote Sensing of Environment*, **140**, 614–624.
- 757 Avitabile V, Herold M, Henry M, Schmillius C (2011) Mapping biomass with remote  
758 sensing: a comparison of methods for the case study of Uganda. *Carbon Balance and*  
759 *Management*, **6**, 7.
- 760 Avitabile V, Baccini A, Friedl MA, Schmillius C (2012) Capabilities and limitations of  
761 Landsat and land cover data for aboveground woody biomass estimation of Uganda.  
762 *Remote Sensing of Environment*, **117**, 366–380.
- 763 Baccini A, Goetz SJ, Walker WS et al. (2012) Estimated carbon dioxide emissions from  
764 tropical deforestation improved by carbon-density maps. *Nature Climate Change*, **2**,  
765 182–185.
- 766 Baccini A, Asner GP (2013) Improving pantropical forest carbon maps with airborne LiDAR  
767 sampling. *Carbon Management*, **4**, 591–600.



- 768 Bartholomé E, Belward a. S (2005) GLC2000: a new approach to global land cover mapping  
769 from Earth observation data. *International Journal of Remote Sensing*, **26**, 1959–1977.
- 770 Bates JM, Granger CWJ (1969) The Combination of Forecasts. *Journal of the Operational*  
771 *Research Society*, **20**, 451–468.
- 772 Birdsey R, Angeles-Perez G, Kurz W a et al. (2013) Approaches to monitoring changes in  
773 carbon stocks for REDD+. *Carbon Management*, **4**, 519–537.
- 774 Breiman L (2001) Random forests. *Machine Learning*, **45**, 5–23.
- 775 Calders K, Newnham G, Burt A et al. (2015) Nondestructive estimates of above-ground  
776 biomass using terrestrial laser scanning. *Methods in Ecology and Evolution*, **6**, 198–208.
- 777 Cartus O, Kellndorfer J, Walker W, Franco C, Bishop J, Santos L, Michel-Fuentes JM (2014)  
778 A National, Detailed Map of Forest Aboveground Carbon Stocks in Mexico. *Remote*  
779 *Sensing*, **6**, 5559–5588.
- 780 Chave J, Olivier J, Bongers F et al. (2008) Above-ground biomass and productivity in a rain  
781 forest of eastern South America. *Journal of Tropical Ecology*, **24**, 355–366.
- 782 DiMiceli CM, Carroll ML, Sohlberg RA et al. (2011) Annual Global Automated MODIS  
783 Vegetation Continuous Fields (MOD44B) at 250 m Spatial Resolution for Data Years  
784 Beginning Day 65, 2000 - 2010, Collection 5 Percent Tree Cover, University of  
785 Maryland, College Park, MD, USA
- 786 ESA (2014a) Global land cover map for the epoch 2005. <http://www.esa-landcover-cci.org/>
- 787 ESA (2014b) Global Water Bodies. <http://www.esa-landcover-cci.org/>
- 788 FAO (2000) Global ecological zoning for the global forest resources assessment 2000. FAO  
789 FRA Working Paper Rome, Italy; 2001
- 790 Feldpausch TR, Banin L, Phillips OL et al. (2011) Height-diameter allometry of tropical  
791 forest trees. *Biogeosciences*, **8**, 1081–1106.

- 792 Feldpausch TR, Lloyd J, Lewis SL et al. (2012) Tree height integrated into pantropical forest  
793 biomass estimates. *Biogeosciences*, **9**, 3381–3403.
- 794 Ge Y, Avitabile V, Heuvelink GBM, Wang J, Herold M (2014) Fusion of pan-tropical  
795 biomass maps using weighted averaging and regional calibration data. *International*  
796 *Journal of Applied Earth Observation and Geoinformation*, **31**, 13–24.
- 797 Goetz S, Dubayah R (2011) Advances in remote sensing technology and implications for  
798 measuring and monitoring forest carbon stocks and change. *Carbon Management*, **2**,  
799 231–244.
- 800 Gonzalez de Tanago J, Bartholomeus H, Joseph S et al. (2015) Terrestrial LiDAR and 3D tree  
801 Quantitative Structure Model for quantification of aboveground biomass loss from  
802 selective logging in a tropical rainforest of Peru. In: *Proceedings of Silvilaser 2015*  
803 *Conference. La Grande Motte, France. 28-30 September 2015*.
- 804 Grace J, Mitchard E, Gloor E (2014) Perturbations in the carbon budget of the tropics. *Global*  
805 *Change Biology*.
- 806 Harris NL, Brown S, Hagen SC et al. (2012) Baseline Map of Carbon Emissions from  
807 Deforestation in Tropical Regions. *Science*, **336**, 1573–1576.
- 808 Hill TC, Williams M, Bloom A, Mitchard ET, Ryan CM (2013) Are Inventory Based and  
809 Remotely Sensed Above-Ground Biomass Estimates Consistent? *PLoS ONE*, **8**, 1–8.
- 810 Houghton RA, House JI, Pongratz J et al. (2012) Carbon emissions from land use and land-  
811 cover change. *Biogeosciences*, **9**, 5125–5142.
- 812 Jiahui W, Zamar R, Marazzi A, et al. (2014) robust: Robust Library. R package version 0.4-  
813 16. <http://CRAN.R-project.org/package=robust>.
- 814 Kearsley E, de Haulleville T, Hufkens K et al. (2013) Conventional tree height-diameter  
815 relationships significantly overestimate aboveground carbon stocks in the Central Congo  
816 Basin. *Nature communications*, **4**, 2269.

- 817 IPCC (2003) Good practice guidance for land use, land-use change and forestry. IPCC  
818 National Greenhouse Gas Inventories Programme, Technical Support Unit. Hayama,  
819 Japan: Institute for Global Environmental Strategies.
- 820 IPCC (2006) 2006 IPCC Guidelines for National Greenhouse Gas Inventories, Prepared by  
821 the National Greenhouse Gas Inventories Programme, Eggleston HS, Buendia L, Miwa  
822 K, Ngara T and Tanabe K (eds). Published: IGES, Japan.
- 823 Langner A, Achard F, Grassi G (2014) Can recent pan-tropical biomass maps be used to  
824 derive alternative Tier 1 values for reporting REDD+ activities under UNFCCC?  
825 *Environmental Research Letters*, **9**, 124008.
- 826 Lewis SL, Lopez-Gonzalez G, Sonké B et al. (2009) Increasing carbon storage in intact  
827 African tropical forests. *Nature*, **457**, 1003–1006.
- 828 Lewis SL, Sonké B, Sunderland T et al. (2013) Above-ground biomass and structure of 260  
829 African tropical forests. *Philosophical transactions of the Royal Society of London.  
830 Series B, Biological sciences*, **368**, 20120295.
- 831 Malhi Y, Wood D, Baker TR et al. (2006) The regional variation of aboveground live biomass  
832 in old-growth Amazonian forests. *Global Change Biology*, **12**, 1107–1138.
- 833 Mitchard ET, Saatchi SS, Baccini A, Asner GP, Goetz SJ, Harris NL, Brown S (2013)  
834 Uncertainty in the spatial distribution of tropical forest biomass: a comparison of pan-  
835 tropical maps. *Carbon balance and management*, **8**, 10.
- 836 Mitchard ET, Feldpausch TR, Brienen RJW et al. (2014) Markedly divergent estimates of  
837 Amazon forest carbon density from ground plots and satellites. *Global Ecology and  
838 Biogeography*, **23**, 935–946.
- 839 Nogueira MA, Diaz G, Andrioli W, Falconi FA, Stangarlin JR (2006) Secondary metabolites  
840 from *Diplodia maydis* and *Sclerotium rolfsii* with antibiotic activity. *Brazilian Journal of  
841 Microbiology*, **37**, 14–16.

- 842 Pan Y, Birdsey RA, Fang J et al. (2011) A large and persistent carbon sink in the world's  
843 forests. *Science*, **333**, 988–993.
- 844 Pearson TRH, Brown S, Casarim FM (2014) Carbon emissions from tropical forest  
845 degradation caused by logging. *Environmental Research Letters*, **034017**, 11.
- 846 Phillips O L, Malhi Y, Higuchi N et al. (1998) Changes in the carbon balance of Tropical  
847 Forests: Evidence from long-term plots. *Science*, **282**, 439–442.
- 848 Phillips OL, Aragão LEOC, Lewis SL et al. (2009) Drought sensitivity of the Amazon  
849 Rainforest. *Science*, **323**, 1344–1347.
- 850 Phillips OL, Lewis SL (2014) Evaluating the tropical forest carbon sink. *Global Change*  
851 *Biology*, **20**, 2039–2041.
- 852 Potapov P, Yaroshenko A, Turubanova S et al. (2008) Mapping the world's intact forest  
853 landscapes by remote sensing. *Ecology and Society*, **13**.
- 854 Romijn E, Herold M, Kooistra L, Murdiyarso D, Verchot L (2012) Assessing capacities of  
855 non-Annex I countries for national forest monitoring in the context of REDD+.  
856 *Environmental Science and Policy*, **19-20**, 33–48.
- 857 Saatchi SS, Harris NL, Brown S et al. (2011) Benchmark map of forest carbon stocks in  
858 tropical regions across three continents. *Proceedings of the National Academy of*  
859 *Sciences*, 108, 9899–9904.
- 860 Saatchi SS, Mascaro J, Xu L et al. (2014) Seeing the forest beyond the trees. *Global Ecology*  
861 *& Biogeography*, **23**, 935 – 946.
- 862 Searle SR (1971) *Linear Models*, Vol. XXI. WILEY-VCH Verlag, York-London-Sydney-  
863 Toronto, 532 pp.
- 864 Simard M, Pinto N, Fisher JB, Baccini A (2011) Mapping forest canopy height globally with  
865 spaceborne lidar. *Journal of Geophysical Research: Biogeosciences*, 116, 1–12.

- 866 Slik JWF, Aiba SI, Brearley FQ et al. (2010) Environmental correlates of tree biomass, basal  
867 area, wood specific gravity and stem density gradients in Borneo's tropical forests.  
868 *Global Ecology and Biogeography*, **19**, 50–60.
- 869 Slik JWF, Paoli G, Mcguire K et al. (2013) Large trees drive forest aboveground biomass  
870 variation in moist lowland forests across the tropics. *Global Ecology and Biogeography*,  
871 **22**, 1261–1271.
- 872 Ter Steege H, Pitman NC a, Phillips OL et al. (2006) Continental-scale patterns of canopy  
873 tree composition and function across Amazonia. *Nature*, **443**, 444–447.
- 874 Willcock S, Phillips OL, Platts PJ et al. (2012) Towards Regional, Error-Bounded Landscape  
875 Carbon Storage Estimates for Data-Deficient Areas of the World. *PLoS ONE*, **7**, 1–10.
- 876 Wright JS (2013) The carbon sink in intact tropical forests. *Global Change Biology*, **19**, 337–  
877 339.
- 878 Ziegler AD, Phelps J, Yuen JQ et al. (2012) Carbon outcomes of major land-cover transitions  
879 in SE Asia: Great uncertainties and REDD+ policy implications. *Global Change*  
880 *Biology*, **18**, 3087–3099.
- 881 Zolkos SG, Goetz SJ, Dubayah R (2013) A meta-analysis of terrestrial aboveground biomass  
882 estimation using lidar remote sensing. *Remote Sensing of Environment*, **128**, 289–298.
- 883
- 884
- 885
- 886
- 887
- 888
- 889
- 890

891 **Supporting Information**

892 **Appendix S1.** Supplementary methods and results

893

894

895

896

897

898

899

900

901

902

903

904

905

906

907

908

909

910

911

912 **Tables**

913 **Table 1: Number of reference data (plots and 1-km pixels) selected after the screening, upscaling and**  
 914 **consolidating procedures, per continent. The reference data selected for each individual dataset are**  
 915 **reported in Table S1. The field plots underpinning the reference AGB maps are not included.**

| Continent         | Available    | Selected     |               | Consolidated  |
|-------------------|--------------|--------------|---------------|---------------|
|                   | <i>Plots</i> | <i>Plots</i> | <i>Pixels</i> | <i>Pixels</i> |
| <b>Africa</b>     | 2,281        | 1,976        | 953           | 953           |
| <b>S. America</b> | 648          | 474          | 449           | 449           |
| <b>C. America</b> | -            | -            | 5,260         | 7,675         |
| <b>Asia</b>       | 3,698        | 1,833        | 353           | 400           |
| <b>Australia</b>  | -            | -            | 5,000         | 5,000         |
| <b>Total</b>      | <b>6,627</b> | <b>4,283</b> | <b>12,015</b> | <b>14,477</b> |

916

917

918

919

920

921

922

923

924

925

926

927

928 **Figure captions**

929 **Figure 1: Flowchart illustrating the methods for generating the fused biomass map and associated**  
930 **uncertainty**

931 **Figure 2: AGB reference dataset for the tropics and spatial coverage of the two input maps**

932 **Figure 3: Fused map, representing the distribution of live woody aboveground biomass (AGB) for all land**  
933 **cover types at 1-km resolution for the tropical region.**

934 **Figure 4: Difference maps obtained by subtracting the fused map from the Saatchi map (a) and the**  
935 **Baccini map (b).**

936 **Figure 5: RMSE (a) and bias (b) of the fused and input maps per continent obtained using independent**  
937 **reference data not used for model development. The error bars indicate one standard deviation of the 100**  
938 **simulations. Numbers reported in brackets indicate the number of reference observations used for each**  
939 **continent. The results for the pan-tropics exclude Australia, which is not covered by the Baccini map.**

940 **Figure 6: scatterplots of the validation reference data (x-axis) and predictions (y-axis) of the input maps**  
941 **(left plots) and fused map (right plots) by continent.**

942 **Figure 7: Uncertainty of the fused map, in absolute values (a) and relative to the AGB estimates (b),**  
943 **representing one standard deviation of the error of the fused map.**

944

945

946

947

948

949

950

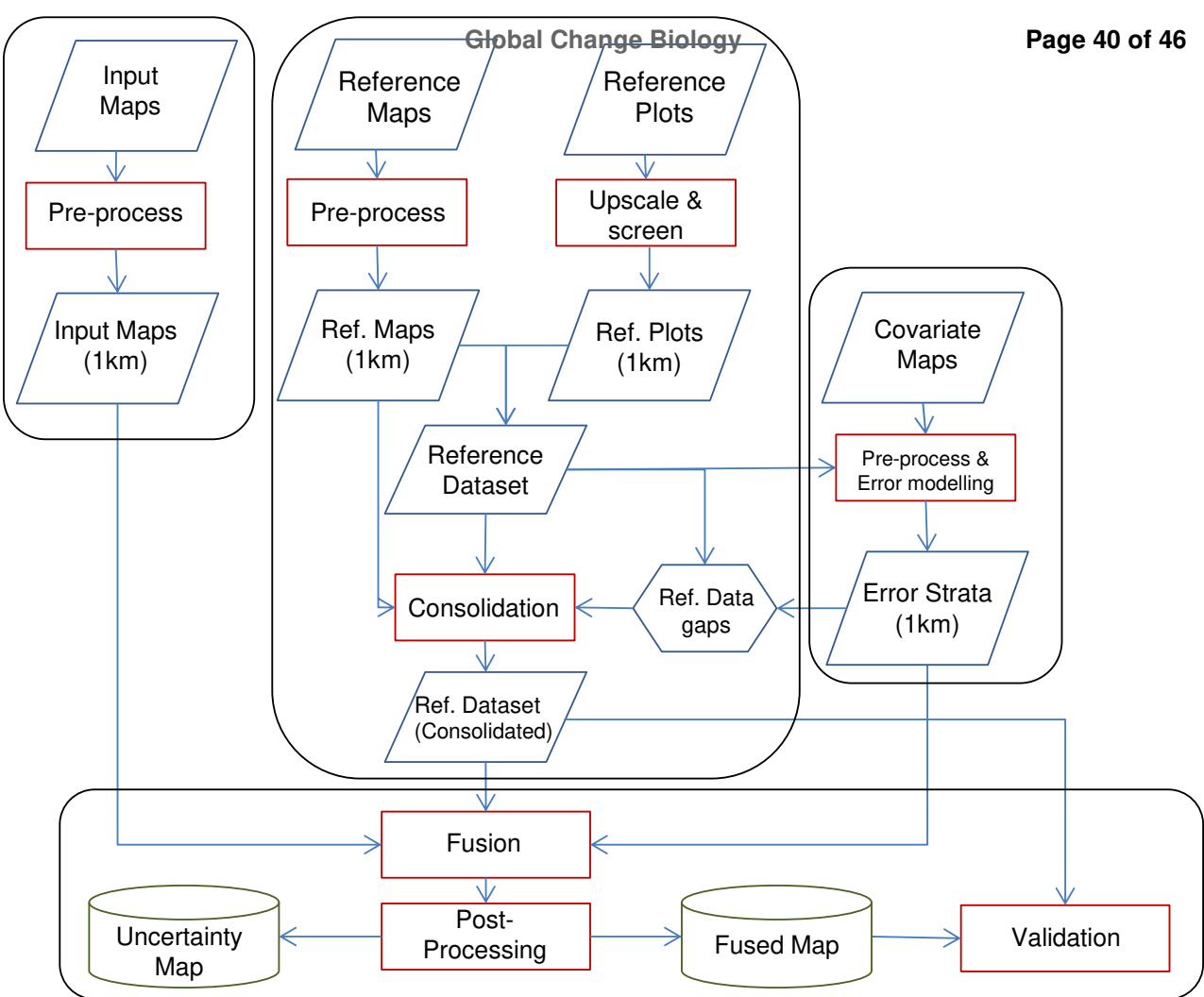
951

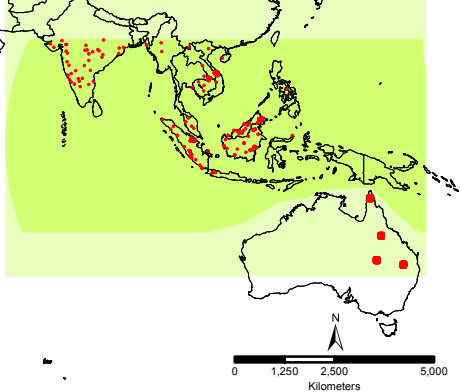
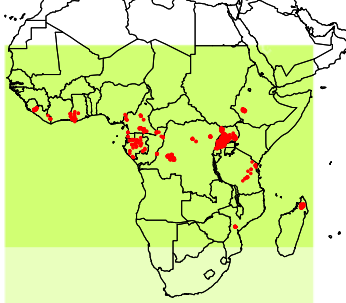
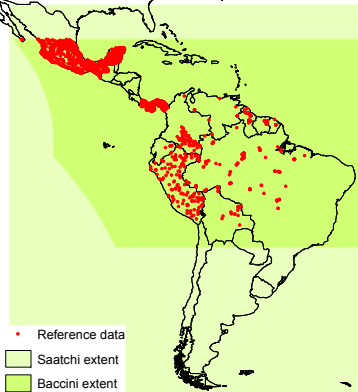
952

953

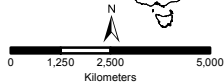
954

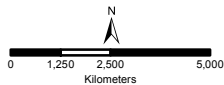
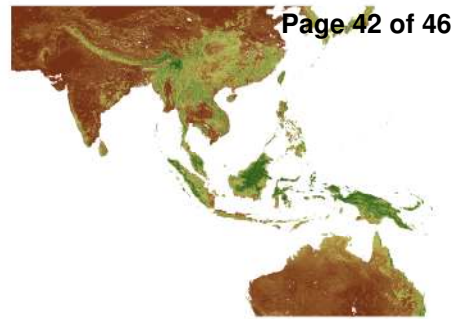
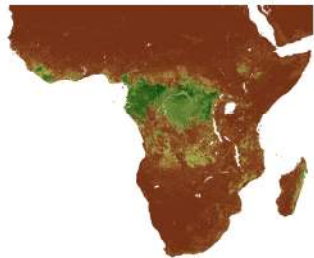
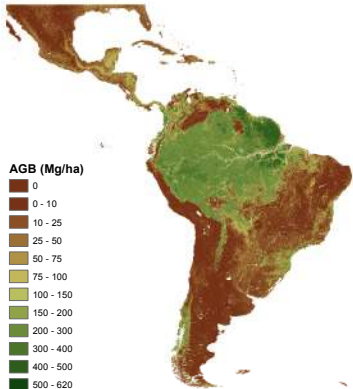


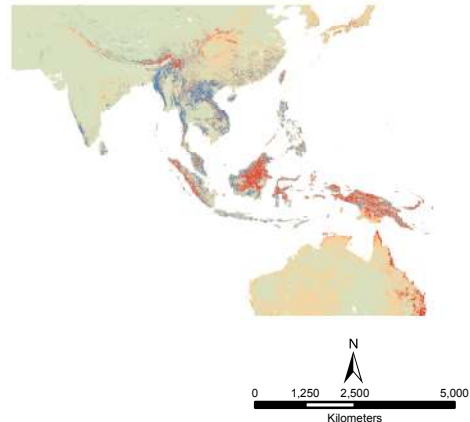
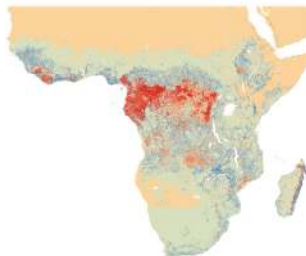
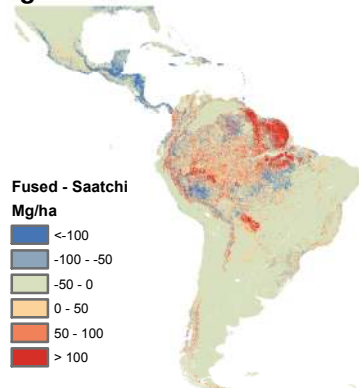




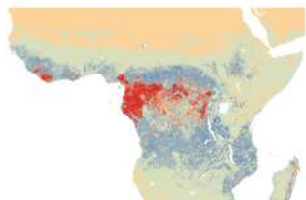
- Reference data
- Saatchi extent
- Baccini extent

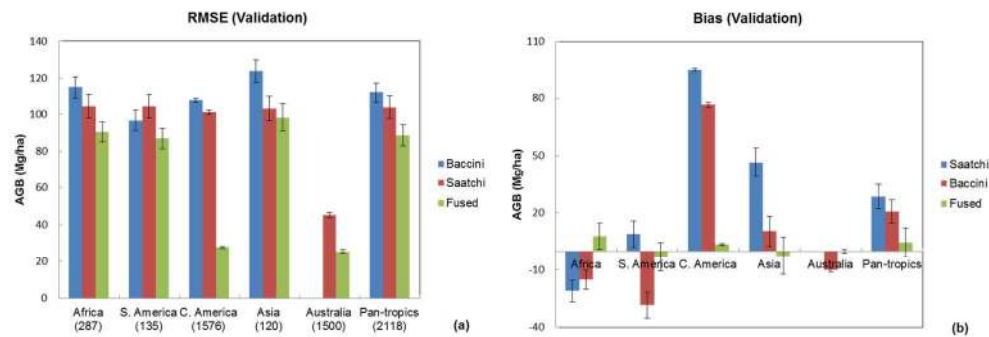




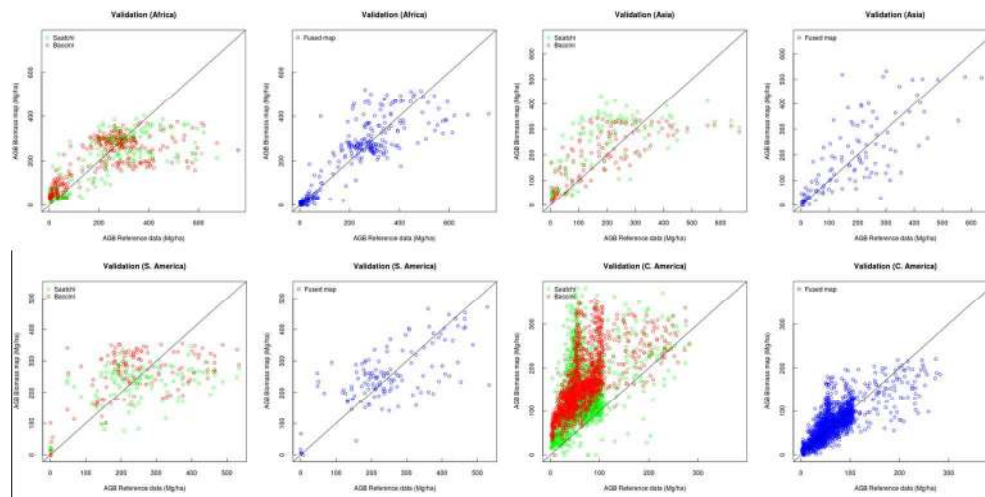


(b)



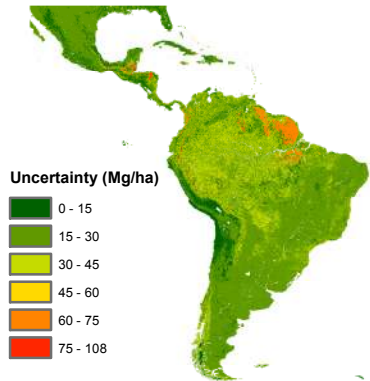


RMSE (a) and bias (b) of the fused and input maps per continent obtained using independent reference data not used for model development. The error bars indicate one standard deviation of the 100 simulations. Numbers reported in brackets indicate the number of reference observations used for each continent. The results for the pan-tropics exclude Australia, which is not covered by the Baccini map.  
469x160mm (96 x 96 DPI)

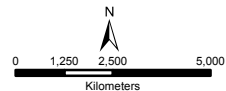
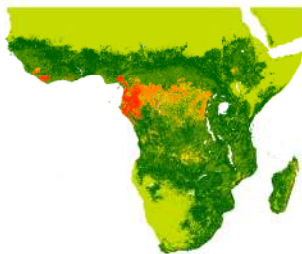
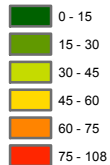


scatterplots of the validation reference data (x-axis) and predictions (y-axis) of the input maps (left plots) and fused map (right plots) by continent.  
311x155mm (150 x 150 DPI)

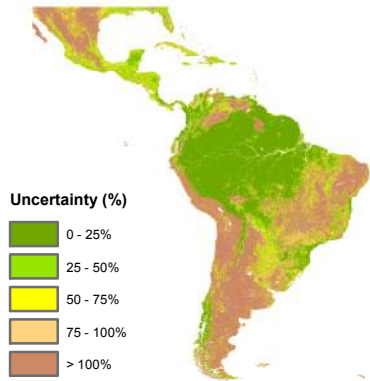
(a)



Uncertainty (Mg/ha)



(b)



Uncertainty (%)

